Draft version March 24, 2024
Typeset using LaTeX **twocolumn** style in AASTeX631

Chemically Self-Consistant Modeling of the Globular Cluster NGC 2808 and its Effects on the Inferred Helium abundance of Multiple Stellar Populations.

Emily M. Boudreaux,[1] Brian C. Chaboyer,[1] Amanda Ash,[2] Renata Edaes Hoh,[1] and Gregory Feiden[2]

[1] *Department of Physics and Astronomy, Dartmouth College, Hanover, NH 03755, USA*
[2] *Department of Physics and Astronomy, University of North Georgia, Dahlonega, GA 30533, USA*

ABSTRACT

The Helium abundances in the multiple populations which are now known to comprise all closely studied Milky Way globular clusters are often inferred by fitting isochohrones generated from stellar evolutionary models to globular cluster photometry. It is therefore important to build stellar models that are chemically self-consistent in terms of their structure, atmosphere, and opacity. In this work we present the first chemically self-consistent stellar models of the Milky Way Globular Cluster NGC 2808 using MARCS model atmospheres, OPLIB high-temperature radiative opacities, and AESOPUS low-temperature radiative opacities. These stellar models were fit to the NGC 2808 photometry using `Fidanka` , a new software tool that was developed optimally fit cluster photometry to isochrones and for population synthesis. `Fidanka` can determine, in a relatively unbiased way, the ideal number of distinct populations which exist within a dataset and then fits isochrones to each population. We achieve this through a combination of Bayesian Gaussian Mixture Modeling and a novel number density estimation algorithm. Using `Fidanka` and F275W-F814W photometry from the Hubble UV Globular Cluster Survey we find that the helium abundance of the second generation of stars in NGC 2808 is higher than the first generation by $15 \pm 3\%$. This is in agreement with previous studies of NGC 2808. **This work, along with previous work by Dotter (2016) focused on NGC 6752 demonstrates that chemically self-consistent models of globular clusters do not signifigantly alter infered helium abundances and are therefor unlikeley to be worth the signifigant additional time investment.**

Keywords: Globular Clusters (656), Stellar evolutionary models (2046)

1. INTRODUCTION

Globular clusters (GCs) are among the oldest observable objects in the universe (Peng et al. 2011). They are characterized by high densities with typical half-light radii of ≤10 pc (van den Bergh 2010), and typical masses ranging from 10^4–10^5 $M_\odot$ (Brodie & Strader 2006) — though some GCs are significantly larger than these typical values (e.g. ω Cen, Richer et al. 1991). GCs provide a unique way to probe stellar evolution (Baumgardt & Makino 2003), galaxy formation models (Boylan-Kolchin 2018; Kravtsov & Gnedin 2005), and dark matter halo structure (Hudson & Robison 2018).

Corresponding author: Emily M. Boudreaux
emily.m.boudreaux.gr@dartmouth.edu,
emily@boudreauxmail.com

The traditional view of Globular Clusters was that they consisted of a single stellar population (SSP, in some publications this is referred to as a Simple Stellar Population). This view was supported by spectroscopically uniform heavy element abundances (Carretta et al. 2010; Bastian & Lardo 2018) across most clusters (M54 and ωCen are notable exceptions, see Marino et al. (2015) for further details), and the lack of evidence for multiple stellar populations (MPs) in past color-magnitude diagrams of GCs (i.e. Sandage 1953; Alcaino 1975). However, over the last 40 years non-trivial star-to-star light-element abundance variations have been observed (i.e. Smith 1987) and, in the last two decades, it has been definitively shown that most if not all Milky Way GCs have MPs (Gratton et al. 2004, 2012; Piotto et al. 2015). The lack of photometric evidence for MPs prior to the 2000, can be attributed to the more narrow color bands available, until very recently, to ground based photometric surveys (Milone et al. 2017).

The prevalence of multiple populations in GCs is so distinct that the proposed definitions for what constitutes a globular cluster now often center the existence of MPs (e.g. Carretta et al. 2010). Whereas, people have have often tried to categorized objects as GCs through relations between half-light radius, density, and surface brightness profile, in fact many objects which are generally thought of as GCs don't cleanly fit into these cuts (Peebles & Dicke 1968; Brown et al. 1991, 1995; Bekki & Chiba 2002). Consequently, Carretta et al. (2010) proposed a definition of GC based on observed chemical inhomogeneities in their stellar populations. The modern understanding of GCs then is not simply one of a dense cluster of stars that may have chemical inhomogeneities and multiple populations; rather, it is one where those chemical inhomogeneities and multiple populations themselves are the defining element of a GC.

All Milky Way globular clusters older than 2 Gyr studied in detail show populations enriched in He, N, and Na while also being deplete in O and C (Piotto et al. 2015; Bastian & Lardo 2018). These light element abundance patterns also are not strongly correlated with variations in heavy element abundance, resulting in spectroscopically uniform Fe abundances between populations. Further, high-resolution spectral studies reveal anti-correlations between N-C abundances, Na-O abundances, and potentially Al-Mg (Sneden et al. 1992; Gratton et al. 2012). Typical stellar fusion reactions can deplete core oxygen; however, the observed abundances of Na, Al, and Mg cannot be explained by the CNO cycle (Prantzos et al. 2007). Consequently, globular cluster populations must be formed by some novel means.

Formation channels for these multiple populations remain a point of debate among astronomers. Most proposed formation channels consist of some older, more massive, population of stars polluting the pristine cluster media before a second population forms, now enriched in heavier elements which they themselves could not have generated (for a detailed review see Gratton et al. 2012). The four primary candidates for these polluters are asymptotic giant branch stars (AGBs, Ventura et al. 2001; D'Ercole et al. 2010), fast rotating massive stars (FRMSs, Decressin et al. 2007), super massive stars (SMSs, Denissenkov & Hartwick 2014), and massive interacting binaries (MIBs, de Mink et al. 2009; Bastian & Lardo 2018).

Hot hydrogen burning (i.e. proton capture), material transport to the surface, and material ejection into the intra-cluster media are features of each of these models and consequently they can all be made to *qualitatively* agree with the observed elemental abundances. However, none of the standard models can currently account for all specific abundances (Gratton et al. 2012). AGB and FRMS models are the most promising; however, both models have difficulty reproducing severe O depletion (Ventura & D'Antona 2009; Decressin et al. 2007). Moreover, AGB and FRMS models require significant mass loss ($\sim 90\%$) between cluster formation and the current epoch — implying that a significant fraction of halo stars formed in GCs (Renzini 2008; D'Ercole et al. 2008; Bastian & Lardo 2015).

In addition to the light-element anti-correlations observed, it is also known that younger populations are significantly enhanced in Helium (Piotto et al. 2007, 2015; Latour et al. 2019). Depending on the cluster, helium mass fractions as high as $Y = 0.4$ have been inferred (e.g Milone et al. 2015a). However, due to both the relatively high and tight temperature range of partial ionization for He and the efficiency of gravitational settling in core helium burning stars, the initial He abundance of globular cluster stars cannot be observed; consequently, the evidence for enhanced He in GCs originates from comparison of theoretical stellar isochrones to the observed color-magnitude-diagrams of globular clusters. Therefore, a careful handling of chemistry is essential when modeling with the aim of discriminating between MPs; yet, only a very limited number of GCs have been studied with chemically self-consistent (structure and atmosphere) isochrones (e.g. Dotter et al. 2015, NGC 6752).

NGC 2808 is the prototype globular cluster to host Multiple Populations. Various studies since 2007 have identified that it may host anywhere from 2-5 stellar populations. These populations have been identified both spectroscopically (i.e. Carretta et al. 2004; Carretta 2006; Carretta et al. 2010; Gratton et al. 2011; Carretta 2015; Hong et al. 2021) and photometrically (i.e. Piotto et al. 2007, 2015; Milone et al. 2015a, 2017; Pasquato & Milone 2019). Note that recent work (Valle et al. 2022) calls into question the statistical significance of the detections of more than 2 populations in the spectroscopic data. Here we present new, chemically self-consistent modeling of the photometry of the two extreme populations of NGC 2808 identified by Milone et al. (2015a), populations A and E. **We do not consider populations B, C, or D identified in Milone et al. (2015a) as the purpose of this work is to identify if chemically self-consistent modelling results in a statisically signifigant deviation in the infered helium abundance when compared to non chemically self-consistent models. Use of the two populations in the NGC 2808 with the highest identified difference be-**

tween their helium populations is sufficent for to answer this question. We use archival photometry from the Hubble UV Globular Cluster Survey (HUGS) (Piotto et al. 2015; Milone et al. 2017) in the F275W and F814W passbands to characterize multiple populations in NGC 2808 (Milone et al. 2015a,b) (This data is avalible at MAST: 10.17909/T9810F). Additionally, we present a likelihood analysis of the photometric data of NGC 2808 to determine the number of populations present in the cluster.

2. CHEMICAL CONSISTENCY

There are three primary areas in which must the stellar models must be made chemically consistent: the atmospheric boundary conditions, the opacities, and interior abundances. The interior abundances are relatively easily handled by adjusting parameters within our stellar evolutionary code. However, the other two areas are more complicated to bring into consistency. Atmospheric boundary conditions and opacities must both be calculated with a consistent set of chemical abundances outside of the stellar evolution code. For evolution we use the Dartmouth Stellar Evolution Program (DSEP) (Dotter et al. 2008), a well tested 1D stellar evolution code which has a particular focus on modelling low mass stars (≤ 2 M$_\odot$)

2.1. *Atmospheric Boundary Conditions*

Certain assumptions, primarily that the radiation field is at equilibrium and radiative transport is diffusive (Salaris & Cassisi 2005), made in stellar structure codes, such as DSEP, are valid when the optical depth of a star is large. However, in the atmospheres of stars, the number density of particles drops low enough and the optical depth consequently becomes small enough that these assumptions break down, and separate, more physically motivated, plasma modeling code is required. Generally structure code will use tabulated atmospheric boundary conditions generated by these specialized codes, such as ATLAS9 (Kurucz 1993), PHOENIX (Husser et al. 2013), MARCS (Gustafsson et al. 2008), and MPS-ATLAS (Kostogryz et al. 2023). Often, as the boundary conditions are expensive to compute, they are not updated as interior abundances vary.

One key element when chemically consistently modeling NGC 2808 modeling is the incorporation of new atmospheric models with the same elemental abundances as the structure code. We use atmospheres generated from the `MARCS` grid of model atmospheres (Plez 2008). `MARCS` provides one-dimensional, hydrostatic, plane-parallel and spherical LTE atmospheric models (Gustafsson et al. 2008). Model atmospheres are made to match the spectroscopically measured elemental abundances of populations A and E. Moreover, for each population, atmospheres with various helium mass fractions are generated. These range from Y=0.24 to Y=0.36 in steps of 0.03. All atmospheric models are computed to an optical depth of $\tau = 100$ where their temperature and pressures serves as boundary conditions for the structure code. In general, enhancing helium in the atmosphere has only a small impact on the atmospheric temperature profile, while leading to a drop in the pressure by $\sim 10 - 20\%$.

2.2. *Opacities*

In addition to the atmospheric boundary conditions, both the high and low temperature opacities used by DSEP must be made chemically consistent. Here we use OPLIB high temperature opacity tables (Colgan et al. 2016) retrieved using the TOPS web-interface. Retrival of High termperature opacities is done using `pyTOPSScrape`, first introduced in Boudreaux & Chaboyer (2023). Low temperature opacity tables are retrieved from the Aesopus 2.0 web-interface (Marigo & Aringer 2009; Marigo et al. 2022). Ideally, these opacities would be the same used in the atmospheric models. However, the opacities used in the MARCS models are not publicly available. As such, we use the opacities provided by the TOPS and Aesopus 2.0 web-interfaces.

3. STELLAR MODELS

We use the Dartmouth Stellar Evolution Program (DSEP, Dotter et al. 2008) to generate stellar models. DSEP is a one-dimensional stellar evolution code which includes a mixing length model of convection, gravitational settling, and diffusion. Using the solar composition presented in (Grevesse et al. 2007) (GAS07), MARCS model atmosphers, OPLIB high temperature opacities, and AESOPUS 2.0 low temperautre opacities we find a solar calibrated mixing length parameter, α_{MLT}, of $\alpha_{MLT} = 1.901$.

We use DSEP to evolve stellar models ranging in mass from 0.3 to 2.0 solar masses from the fully convective pre-main sequence to the tip of the red giant branch. Below 0.7 $M_\odot$ we evolve a model every 0.03 $M_\odot$ and above 0.7 $M_\odot$ we evolve a model every 0.05 $M_\odot$. We evolve models over a grid of mixing length parameters from $\alpha_{MLT} = 1.0$ to $\alpha_{MLT} = 2.0$ in steps of 0.1. For each mixing length, a grid of models and isochrones were calculated, with chemical compositions consistent with Populations A and E (see Tables 1 and 1) and a range of helium abundances (Y=0.24, 0.27, 0.30, 0.33, 0.36, and 0.39). In total,144 sets of isochrones, each with a unique composition and mixing length were calculated.

Each model is evolved in DSEP with typical numeric tolerences of one part in 10^7. Each model is allowed a maximum time step of 50 Myr.

For each combination of population, Y, and α_{MLT} we use the isochrone generation code first presented in Dotter (2016) to generate a grid of isochrones. The isochrone generation code identified equivalent evolutionary points (EEPs) over a series of masses and interpolates between them. The grid of isochrones generated for this work is avalible as a digital supplement to this paper 10.5281/zenodo.10631439. Given the complexity of the parameter space when fitting multiple populations along with the recent warnings in the liteerature regarding overfitting datasets (e.g. Valle et al. 2022) we want to develop a more objective way of fitting isochrones to photometry than if we were to mark median ridge line positions by hand.

4. FIDANKA

When fitting isochrones to the clusters with multiple populations we have four main criteria for any method

- The method must be robust enough to work along the entire main sequence, turn off, and much of the subgiant and red giant branch.
- Any method should consider photometric uncertainty in the fitting process.
- The method should be model independent, weighting any n number of populations equally.
- The method should be automated and require minimal intervention from the user.

We do not believe that any currently available software is a match for our use case. Therefore, we elect to develop our own software suite, `Fidanka` . `Fidanka` is a python package designed to automate much of the process of measuring fiducial lines in CMDs, adhering to the four criteria we lay out above. Primary features of `Fidanka` may be separated into three categories: fiducial line measurement, stellar population synthesise, and isochrone optimization/fitting. Additionally, there are utility functions that are detailed in the `Fidanka` documentation.

4.1. *Fiducial Line Measurement*

`Fidanka` takes a iterative approach to measuring fiducial lines, the first step of which is to make a "guess" as to the fiducial line. This initial guess is calculated

Table 1. Population Composition

Element	Pop A	Pop E	Element	Pop A	Pop E
Li	-0.08	—	In	-1.46	—
Be	0.25	—	Sn	-0.22	—
B	1.57	—	Sb	-1.25	—
C	6.87	5.91	Te	-0.08	—
N	6.42	6.69	I	-0.71	—
O	7.87	6.91	Xe	-0.02	—
F	3.43	—	Cs	-1.18	—
Ne	7.12	6.7	Ba	1.05	—
Na	5.11	5.7	La	-0.03	—
Mg	6.86	6.42	Ce	0.45	—
Al	5.21	6.61	Pr	-1.54	—
Si	6.65	6.77	Nd	0.29	—
P	4.28	—	Pm	-99.0	—
S	6.31	5.89	Sm	-1.3	—
Cl	-1.13	4.37	Eu	-0.61	—
Ar	5.59	5.17	Gd	-1.19	—
K	3.9	—	Tb	-1.96	—
Ca	5.21	—	Dy	-1.16	—
Sc	2.02	—	Ho	-1.78	—
Ti	3.82	—	Er	-1.34	—
V	2.8	—	Tm	-2.16	—
Cr	4.51	—	Yb	-1.42	—
Mn	4.3	—	Lu	-2.16	—
Fe	6.37	—	Hf	-1.41	—
Co	3.86	—	Ta	-2.38	—
Ni	5.09	—	W	-1.41	—
Cu	3.06	—	Re	-2.0	—
Zn	2.3	—	Os	-0.86	—
Ga	0.78	—	Ir	-0.88	—
Ge	1.39	—	Pt	-0.64	—
As	0.04	—	Au	-1.34	—
Se	1.08	—	Hg	-1.09	—
Br	0.28	—	Tl	-1.36	—
Kr	0.99	—	Pb	-0.51	—
Rb	0.26	—	Bi	-1.61	—
Sr	0.61	—	Po	-99.0	—
Y	1.08	—	At	-99.0	—
Zr	1.45	—	Rn	-99.0	—
Nb	-0.8	—	Fr	-99.0	—
Mo	-0.38	—	Ra	-99.0	—
Tc	-99.0	—	Ac	-99.0	—
Ru	-0.51	—	Th	-2.2	—
Rh	-1.35	—	Pa	-99.0	—
Pd	-0.69	—	U	-2.8	—

Note—Relative Metal composition used where a(H) = 12. Where the relative composition is the the same for both populations A and E it is only listed in the population A colum for the sake of visual clarity.

References—Milone et al. (2015a)

Table 2. Population Abundance Ratios

Population	[Fe/H]	[α/Fe]	[C/Fe]	[N/Fe]	[O/Fe]	[r/Fe]	[s/Fe]	C/O	X	Y	Z
A	-1.13	0.32	-0.43	-0.28	0.31	-1.13	-1.13	0.10	0.7285	0.2700	0.00154
E	-1.13	-0.11	-1.39	-0.02	-0.66	-1.13	-1.13	0.10	0.7594	0.240	0.00063

Note—Abundance Ratios for populations A and E in NGC 2808.

References—Milone et al. (2015a)

by splitting the CMD into magnitude bins, with uniform numbers of stars per bin (so that bins are cover a small magnitude range over densely populated regions of the CMD while covering a much larger magnitude range in sparsely populated regions of the CMD, such as the RGB). A unimodal Gaussian distribution is then fit to the color distribution of each bin, and the resulting mean color is used as the initial fiducial line guess. This rough fiducial line will approximately trace the area of highest density. The initial guess will be used to verticalze the CMD so that further algorithms can work in 1-D magnitude bins without worrying about weighting issues caused by varying projections of the evolutionary sequence onto the magnitude axis. Verticalization is preformed taking the difference between the guess fiducial line and the color of each star in the CMD.

If `Fidanka` were to simply apply the same algorithm to the verticalized CMD then the resulting fiducial line would likely be a re-extraction of the initial fiducial line guess. To avoid this, we take a more robust, number density based approach, which considers the distribution of stars in both color and magnitude space simultaneously. For each star in the CMD we first using an `introselect` partitioning algorithm to select the 50 nearest stars in F814W vs. F275W-F814W space. To account for the case where the star is at an extreme edge of the CMD, those 50 stars include the star itself (such that we really select 49 stars + 1). We use `qhull`[1](Barber et al. 1996) to calculate the convex hull of those 50 points. The number density at each star then is defined as $50/A_{hull}$, where A_{hull} is the area of the convex hull. Because we use a fixed number of points per star, and a partitioning algorithm as opposed to a sorting algorithm, this method scales like $\mathcal{O}(n)$, where n is the number of stars in the CMD. This method also intrinsically weights the density of of each star equally as the counting statistics per bin are uniform. We are left with a CMD where each star has a defined number density (Figure 1).

`Fidanka` can now exploit this density map to fit a better fiducial line to the data, as the density map is far more robust to outliers. There are multiple algorithms we implement to fit the fiducial line to the color-density profile in each magnitude bin (Figure 2); they are explained in more detail in the `Fidanka` documentation. However, of most relevance here is the Bayesian Gaussian Mixture Modeling (BGMM) method. BGMM is a clustering algorithm which, for some fixed number of n-dimensional Gaussian distributions, K, determines the mean, covariance, and mixing probability (somewhat analogous to amplitude) of each k^{th} distribution, such that the local lower bound of the likelyhood of each star belonging strongly to a single distribution is maximized.

Maximization is preformed using the Dirichlet process, which is a non-parametric Bayesian method of determining the number of Gaussian distributions, K, which best fit the data (Ferguson 1973; Pedregosa et al. 2011). Use of the Dirichlet process allows for dynamic variation in the number of inferred populations from magnitude bin to magnitude bin. Specifically, populations are clearly visually separated from the lower main sequence through the turn off; however, at the turn off and throughout much of the subgiant branch, the two visible populations overlap due to their extremely similar ages (i.e. Jordán et al. 2002). The Dirichlet process allows for the BGMM method to infer a single population in these regions, while inferring two populations in regions where they are clearly separated. More generally, the use of the Dirichlet process removes the need for a prior on the exact number of populations to fit. Rather, the user specifies a upper bound on the number of populations within the cluster. An example bin (F814W = 20.6) is shown in Figure 3.

`Fidanka` 's BGMM method first breaks down the verticalized CMD into magnitude bins with uniform numbers of stars per bin (here we adopt 250). Any stars left over are placed into the final bin. For each bin a BGMM model with a maximum of 5 populations is fit

[1] https://www.qhull.com

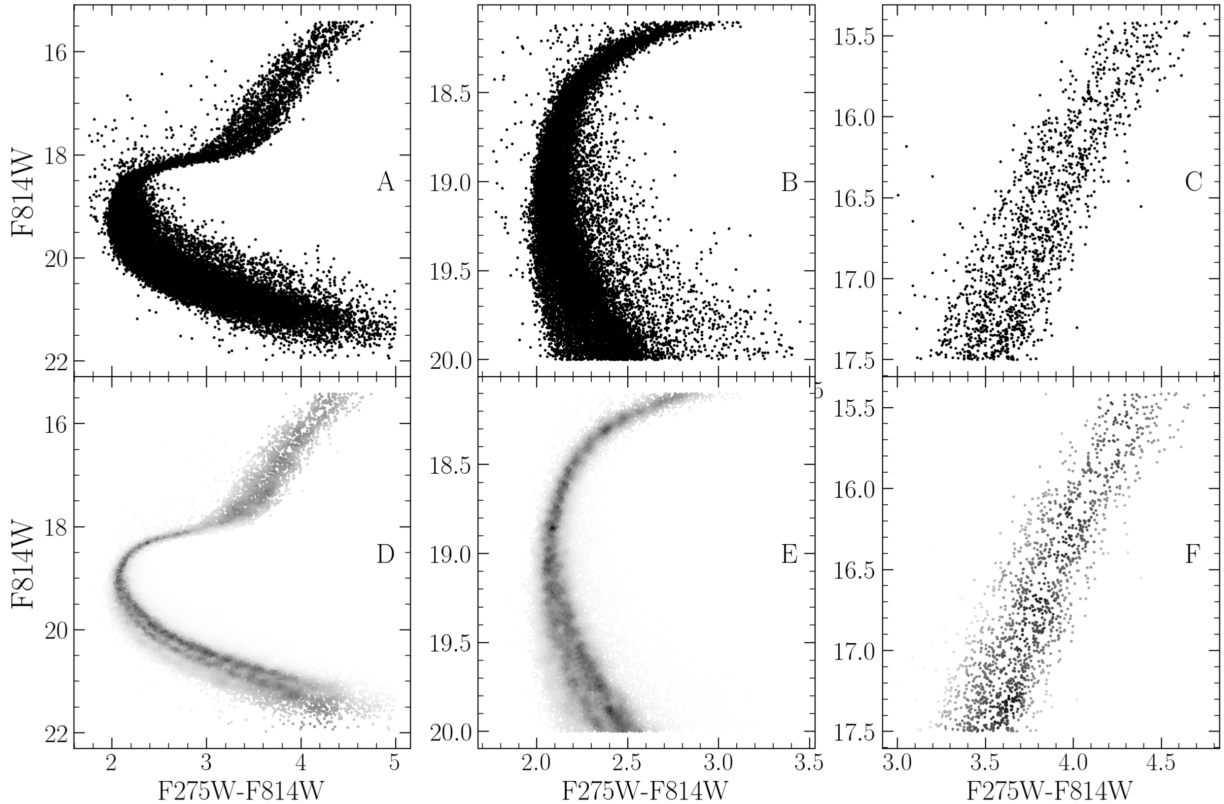

Figure 1. Density map demo showing density estimate over different parts of the evolutionary sequence. The left panel shows the density map over the entire evolutionary sequence, while the middle panel shows the density map over the main sequence and the right most panel shows the density map over the RGB. Figures in the top row are the raw CMD, while figures in the bottom row are colored by the density map.

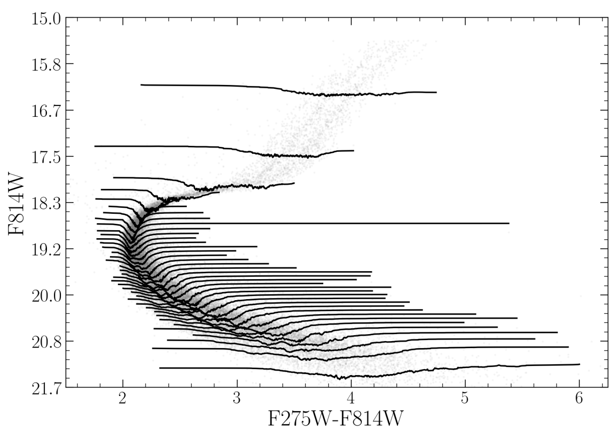

Figure 2. CMD where point brightness is determined by local density. Lines show the density-color profile in each magnitude bin. In this figure adaptive binning targeted 1000 stars per bin

to the color density profile. The number of populations is then inferred from the weighting parameter (the mixing probability) of each population. If the weighting parameter of any k^{th} components less than 0.05, then that component is considered to be spurious and removed. Additionally, if the number of populations in the bin above and the bin below are the same, then the number of populations in the current bin is forced to be the same as the number of populations in the bin above. Finally, the initial guess fiducial line is added back to the BGMM inferred line. Figure 4 shows the resulting fiducial line(s) in each magnitude bin for both a verticalized CMD and a non verticalized CMD. In contrast to other work in the literature where evidence for up to 5 distinct populations has been found; we only find evidence for two stellar populations.

This method of fiducial line extraction effectively discriminated between multiple populations along the main sequence and RGB of a cluster, while simultaneously allowing for the presence of a single population along the MSTO and subgiant branch.

We can adapt this density map based BGMM method to consider photometric uncertainties by adopting a simple Monte Carlo approach. Instead of measuring the fiducial line(s) a single time, `Fidanka` can measure the fiducial line(s) many times, resampling the data with replacement each time. For each resampling `Fidanka` adds a random offset to each filter based on the photometric

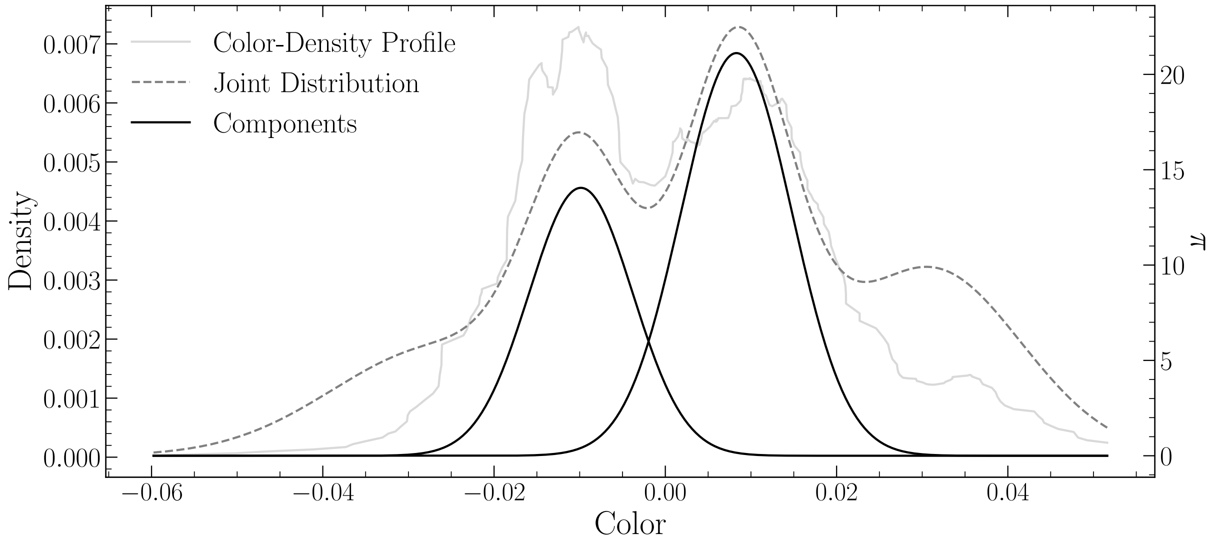

Figure 3. Example of BGMM fit to a magnitude bin. The grey line shows the underlying color-density profile, while the black dashed-line shows the joint distribution of each BGMM component. The solid black lines show the two selected components.

uncertainties of each star. From these n measurements the mean fiducial line for each sequence can be identified along with upper and lower bound confidence intervals in each magnitude bin.

4.2. *Stellar Population Synthesis*

While not extensively used in this paper `Fidanka` can, in addition to measuring fiducial lines, preform stellar population synthesise. `Fidanka` 's population synthesis module can generate synthetic stellar population from a set of MIST formatted isochrones. This is of primary importance for binary population modeling. The module is also used to generate synthetic CMDs for the purpose of testing the fiducial line extraction algorithms against priors.

`Fidanka` uses MIST formatted isochrones (Dotter 2016) as input along with distance modulus, B-V color excess, binary mass fraction, and bolometric corrections. An arbitrarily large number of isochrones may be used to define an arbitrary number of populations. Synthetic stars are samples from each isochrone based on a definable probability (for example it is believed that $\sim 90\%$ of stars in globular clusters are younger population (e.g. Suntzeff & Kraft 1996; Carretta 2013)). Based on the metallicity, μ, and E(B-V) of each isochrone, bolometric corrections are taken from bolometric correction tables. Where bolometric correction tables do not include exact metallicities or extinctions a linear interpolation is preformed between the two bounding values.

4.3. *Isochrone Optimization*

The optimization routines in `Fidanka` will find the best fit distance modulus, B-V color excess, and binary number fraction for a given set of isochrones. If a single isochrone is provided then the optimization is done by minimizing the χ^2 of the perpendicular distances between an isochrone and a fiducial line. If multiple isochrones are provided then those isochrones are first used to run stellar population synthesis and generate a synthetic CMD. The optimization is then done by minimizing the χ^2 of both the perpendicular distances between and widths of the observed fiducial line and the fiducial line of the synthetic CMD.

4.4. *Fidanka Testing*

In order to validate fidanka we have run an series of injection recovery tests using `Fidanka` 's population synthesis routines to build various synthetic populations and `Fidanka` 's fiducial measurement routines to recover these populations. Each population was generated using the initial mass function given in (Milone et al. 2012) for the redmost population ($\alpha = -1.2$). Further, every population was given a binary population fraction of 10%, distance uniformly sampled between 5000pc and 15000pc, and a B-V color excess uniformly sampled between 0 and 0.1. Finally, each synthetic population was generated using a fixed age uniformlly sampled between 7 Gyr and 14 Gyr. An example synthetic population along with its associated best fit isochrone are shown in Figure 5.

For each trial we use `Fidanka` to measure the fiducial line and then optimize that fiducial line against the originating isochrone to esimate distance modulus, age, and color B-V excess. Figure 6 is built from 1000 runs of these trials and show the mean and width of the percent error distributions for μ, $E(B-V)$, and age. In general

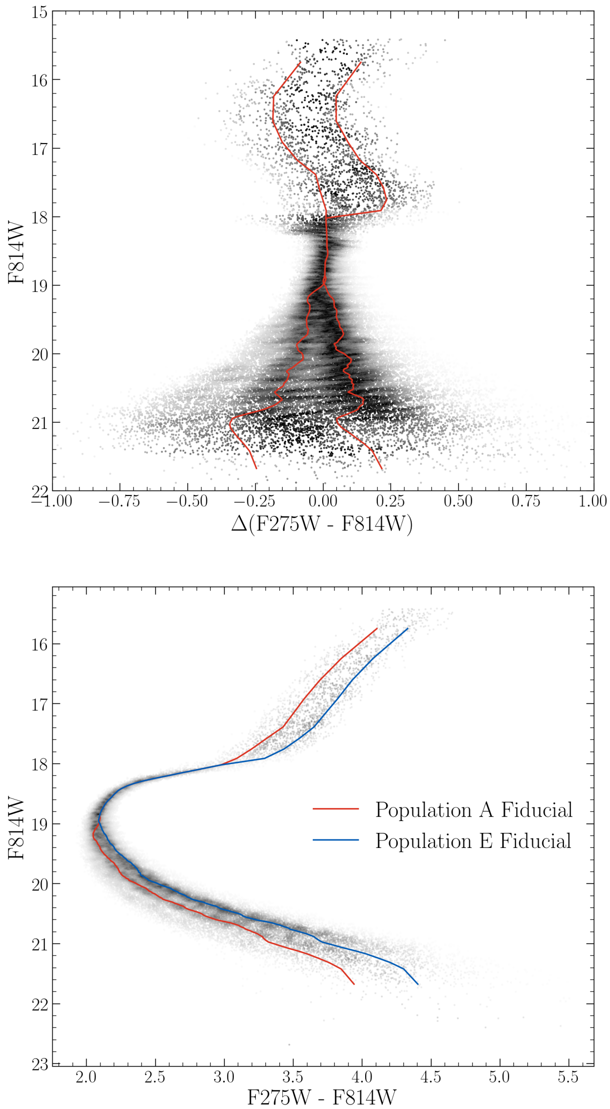

Figure 4. Verticalized CMD where point brightness is determined by density (top). CMD where point brightness is determined by density, calculated fiducial lines are shown (bottom). The data used is from the Hubble Space Telescope UV Legacy Survey of Galactic Globular Clusters.

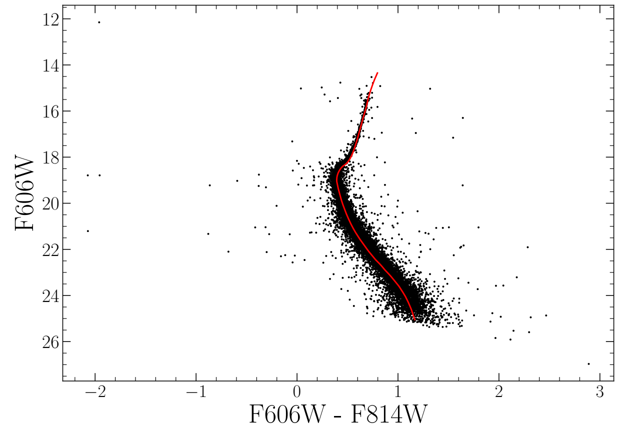

Figure 5. Synthetic population generated by fidanka at 10000pc with E(B-V) = 0, and an age of 12 Gyr along with the best fitting isochrone. The best fit paremeters are derived to be $mu = 15.13$, E(B-V)=0.001, and an age of 12.33 Gyr.

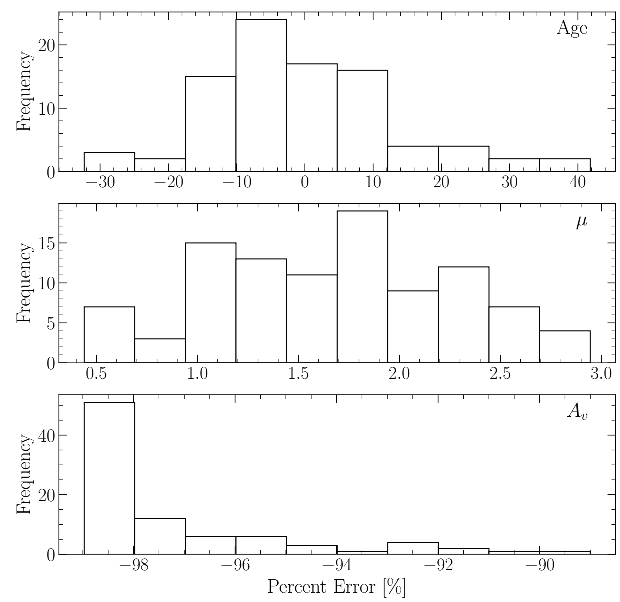

Figure 6. Percent Error distribution for each of the three deriver parameters. Note that these values will be sensitive to the magnitude uncertainties of the photometry. Here we made use of the ACS artificial star tests to estimate the uncertanties.

`Fidanka` is able to recover distance modulii effectively with age and E(B-V) reovery falling in line with other literature that does not cosider the CMD outside of the main sequence, main sequence turn off, sub giant, and red giant branches; specifically, it should be noted that `Fidanka` is not setup to model the horizontal branch.

5. ISOCHRONE FITTING

We fit pairs of isochrones to the HUGS data for NGC 2808 using `Fidanka` , as descrbed in §4. Two isochrones, one for Population A and one for Population E are fit simultaneously. These isochrones are constrained to have distance modulus, μ, and color excess, E(B-V) which agree to within 0.5% and an ages which agree to within 1%. Moreover, we constrain the mixing length, α_{ML}, for any two isochrones in a set to be within 0.5 of one and other. For every isochrone in the set of combination of which fulfilling these constraints μ, $E(B-V)$, Age$_A$, and $\underline{Age_B}$ are optimized to reduce the χ^2 distance ($\chi^2 = \sum\sqrt{\Delta\text{color}^2 + \Delta\text{mag}^2}$) between the fiducial lines and the isochrones. Because we fit fiducial lines directly, we do not need to consider the binary population fraction, f_{bin}, as a free parameter.

The best fit isochrones are shown in Figure 7 and optimized parameters for these are presented in Table 1. We find helium mass fractions that are consistent with those identified in past literature (e.g. Milone et al. 2015a). Note that our helium mass fraction grid has a spacing of 0.03 between grid points and we are therefore unable to resolve between certain proposed helium mass fractions for the younger sequence (for example between 0.37 and 0.39).

Past literature (e.g. Milone et al. 2015a, 2018) have found helium mass fraction variation from the low redmost to bluemost populations of ~ 0.12. Here we find a helium mass fraction variation of 0.15 which, given the spacing of the helium grid we use **is consistent with these past results**.

5.1. *The Number of Populartions in NGC 2808*

In order to estimate the number of populations which ideally fit the NGC 2808 F275W-F814W photometry without overfitting the data we make use of silhouette analysis (Rousseeuw 1987, and in a similar manner to how Valle et al. (2022) preform their analysis of spectroscopic data). We find the average silhouette score for all tagged clusters identified using BGMM in all magnitude bins over the CMD using the standar python module `sklearn`. Figure 8 shows the silhouette analysis results and that two populations fit the photometry most ideally. This is in line with what our BGMM model predicts for the majority of the the CMD.

While we make use a purley CMD based approach in this work, other literature has made use of Chromosome Maps. These consist of implicitly verticalized pseudo colors. In the chromosome map for NGC 2808 there may be evidence for more than two populations; however, the process of transforming magnitude measurements into chromosome space results in dramatically increased uncertanties for each star. We find a mean fractional uncertantie for chromosome parameters of ≈ 1 when starting with magnutude measurements having a mean best-case (i.e. uncertainty assumed to only be due to Poisson statistics) fractional uncertainty of ≈ 0.0005. Because of how `Fidanka` operates, i.e. resampling a probabilty distribution for each star in order to idenfify clusters, we are unable to make statisitcally meaningful statements from the chromosome map

5.2. *ACS-HUGS Photometric Zero Point Offset*

The Hubble legacy archive photometry used in this work is calibrated to the Vega magnitude system. However, we have found that the photometry has a systematic offset of ~ 0.026 magnitudes in the F814W band when compared to the same stars in the ACS survey (Figure 9). The exact cause of this offset is unknown, but it is likely due to a difference in the photometric zero point between the two surveys. A full correction of this offset would require a careful re-reduction of the HUGS photometry, which is beyond the scope of this work. We instead recognize a 0.02 inherent uncertainty in the inferred magnitude of any fit when comparing to the ACS survey. This uncertainty is small when compared to the uncertainty in the distance modulus and should not affect the conclusion of this paper.

The oberved photometric offset between ACS and HUGS reductions introduces a systematic uncertainity when comparing parameters derived from isochrone fits to ACS data vs those fit to HUGS data. Specifically, this offset introduces a $\sim 2Gyr$ uncertainity when comparing ages between ACS and HUGS. Moreover, for two isochrone of the same age, only seperated by helium mass fraction, a shift of the main sequence turn off of is also expected. Figure 10 shows this shift. Note a change in the helium mass fraction of a model by 0.03 results in an approximate 0.08 magnitude shift to the main sequence turn off location. This means that the mean 0.026 magnitude offset we find in between ACS and HUGS data corresponds to an additional approaximate 0.01 uncertainity in the derived helium mass fraction when comparing between these two datasets.

6. CONCLUSION

Here we have preformed the first chemically self-consistent modeling of the Milky Way Globular Cluster NGC 2808. We find that, updated atmospheric boundary conditions and opacity tables do not have a significant effect on the inferred helium abundances of multiple populations. Specifically, we find that population has a helium mass fraction of 0.24, while population E has a helium mass fraction of 0.39. Additionally, we find that the ages of these two populations agree within uncertainties. Further, we only find evidence for two distinct stellar populations, which is in agreement with recent work studying the number of populations in NGC 2808 spectroscopic data.

Further, we introduce a new software suite for globular cluster science, `Fidanka` , which has been released under a permissive open source license. `Fidanka` aims to provide a statistically robust set of tools for estimating the parameters of multiple populations within globular clusters.

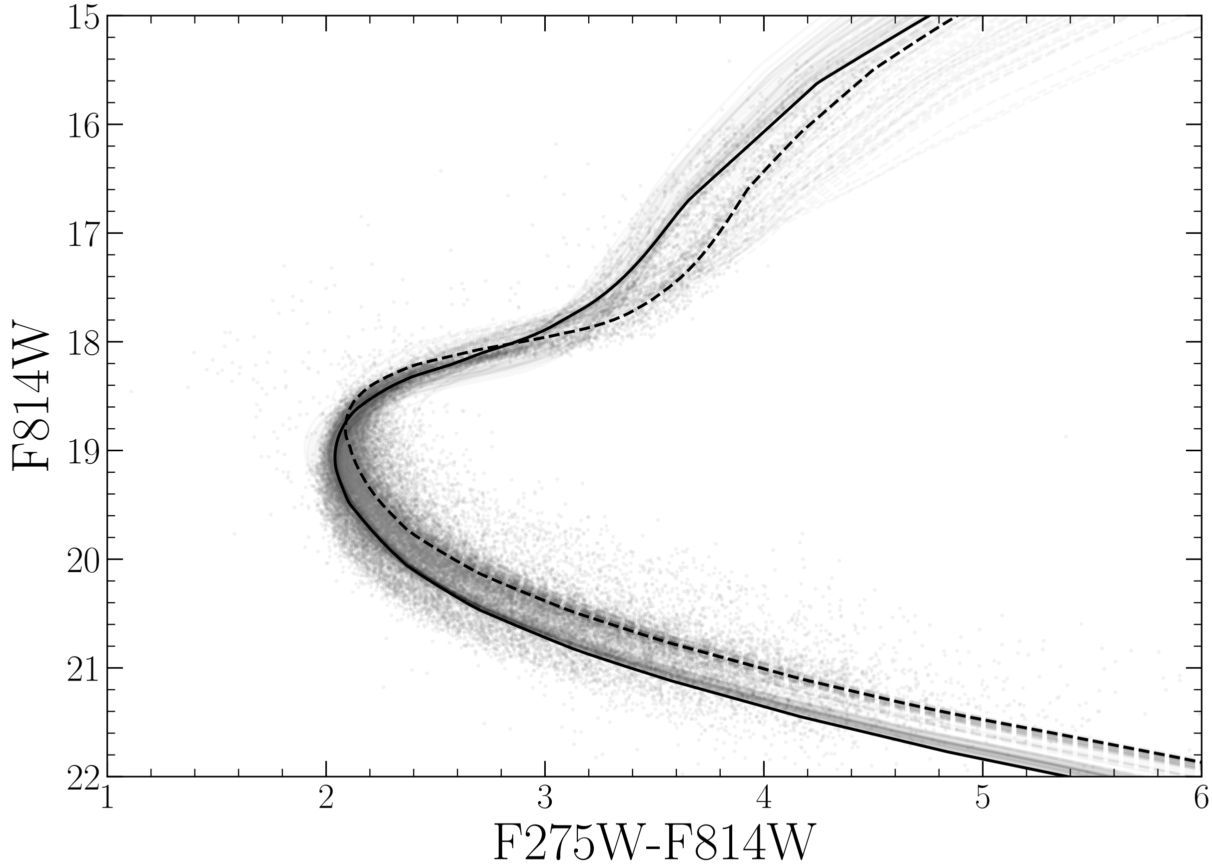

Figure 7. Best fit isochrone results for NGC 2808. The best fit population A and E models are shown as black lines. The following 50 best fit models are presented as grey lines. The solid black line is fit to population A, while the dashed black line is fit to population E.

Population	Age [Gyr]	Distance Modulus	Extinction [mag]	Y	α_{ML}	χ^2_ν
A	$12.996^{+0.87}_{-0.64}$	15.021	0.54	0.24	2.050	0.021
E	$13.061^{+0.86}_{-0.69}$	15.007	0.537	0.39	1.600	0.033

Table 1. Best fit parameters derived from fitting isochrones to the fiducual lines derived from the NCG 2808 photometry. The one sigma uncertainty reported on population age were determined from the 16th and 84th percentiles of the distribution of best fit isochrones ages.

This work has made use of the NASA astrophysical data system (ADS). We would like to thank Elisabeth Newton and Aaron Dotter for their support and for useful disscusion related to the topic of this paper. Additionally, we would like to thank Kara Fagerstrom, Aylin Garcia Soto, and Keighley Rockcliffe for their useful disscusion related to in this work. We acknowledge the support of a NASA grant (No. 80NSSC18K0634).

REFERENCES

Alcaino, G. 1975, A&AS, 21, 15

Barber, C. B., Dobkin, D. P., & Huhdanpaa, H. 1996, ACM Transactions on Mathematical Software (TOMS), 22, 469

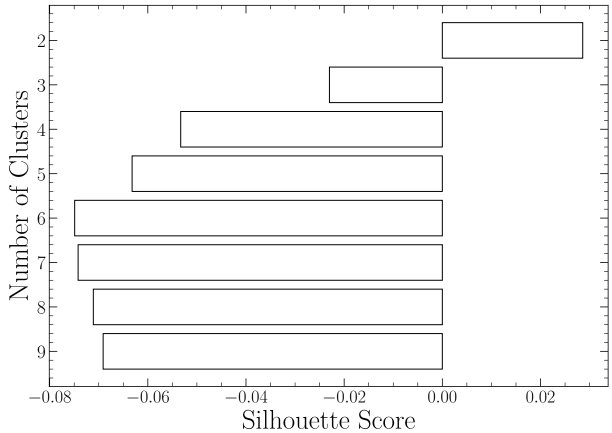

Figure 8. Silhouette analysis for NGC 2808 F275W-F814W photometry. The Silhouette scores are an average of score for each magnitude bin. Positive scores incidate that the clustering algorithm produced well distinguised clusters while negative scores indicate clusters which are not well distinguised.

Bastian, N., & Lardo, C. 2015, MNRAS, 453, 357, doi: 10.1093/mnras/stv1661

Bastian, N., & Lardo, C. 2018, Annual Review of Astronomy and Astrophysics, 56, 83

Baumgardt, H., & Makino, J. 2003, MNRAS, 340, 227, doi: 10.1046/j.1365-8711.2003.06286.x

Bekki, K., & Chiba, M. 2002, The Astrophysical Journal, 566, 245, doi: 10.1086/337984

Boudreaux, E. M., & Chaboyer, B. C. 2023, ApJ, 944, 129, doi: 10.3847/1538-4357/acb685

Boylan-Kolchin, M. 2018, MNRAS, 1423, doi: 10.1093/mnras/sty1490

Brodie, J. P., & Strader, J. 2006, Annu. Rev. Astron. Astrophys., 44, 193

Brown, J. H., Burkert, A., & Truran, J. W. 1991, ApJ, 376, 115, doi: 10.1086/170260

—. 1995, ApJ, 440, 666, doi: 10.1086/175304

Carretta, E. 2006, AJ, 131, 1766, doi: 10.1086/499565

—. 2013, A&A, 557, A128, doi: 10.1051/0004-6361/201322103

—. 2015, ApJ, 810, 148, doi: 10.1088/0004-637X/810/2/148

Carretta, E., Bragaglia, A., & Cacciari, C. 2004, ApJL, 610, L25, doi: 10.1086/423034

Carretta, E., Bragaglia, A., Gratton, R. G., et al. 2010, Astronomy & Astrophysics, 516, A55

Colgan, J., Kilcrease, D. P., Magee, N. H., et al. 2016, in APS Meeting Abstracts, Vol. 2016, APS Division of Atomic, Molecular and Optical Physics Meeting Abstracts, D1.008

de Mink, S. E., Pols, O. R., Langer, N., & Izzard, R. G. 2009, A&A, 507, L1, doi: 10.1051/0004-6361/200913205

Decressin, T., Meynet, G., Charbonnel, C., Prantzos, N., & Ekström, S. 2007, A&A, 464, 1029, doi: 10.1051/0004-6361:20066013

Denissenkov, P. A., & Hartwick, F. D. A. 2014, MNRAS, 437, L21, doi: 10.1093/mnrasl/slt133

D'Ercole, A., D'Antona, F., Ventura, P., Vesperini, E., & McMillan, S. L. W. 2010, MNRAS, 407, 854, doi: 10.1111/j.1365-2966.2010.16996.x

D'Ercole, A., Vesperini, E., D'Antona, F., McMillan, S. L. W., & Recchi, S. 2008, MNRAS, 391, 825, doi: 10.1111/j.1365-2966.2008.13915.x

Dotter, A. 2016, ApJS, 222, 8, doi: 10.3847/0067-0049/222/1/8

Dotter, A., Chaboyer, B., Jevremović, D., et al. 2008, The Astrophysical Journal Supplement Series, 178, 89

Dotter, A., Ferguson, J. W., Conroy, C., et al. 2015, MNRAS, 446, 1641, doi: 10.1093/mnras/stu2170

Ferguson, T. S. 1973, The annals of statistics, 209

Gratton, R., Sneden, C., & Carretta, E. 2004, ARA&A, 42, 385, doi: 10.1146/annurev.astro.42.053102.133945

Gratton, R. G., Carretta, E., & Bragaglia, A. 2012, Astronomy and Astrophysics Reviews, 20, 50, doi: 10.1007/s00159-012-0050-3

Gratton, R. G., Lucatello, S., Carretta, E., et al. 2011, A&A, 534, A123, doi: 10.1051/0004-6361/201117690

Grevesse, N., Asplund, M., & Sauval, A. J. 2007, SSRv, 130, 105, doi: 10.1007/s11214-007-9173-7

Gustafsson, B., Edvardsson, B., Eriksson, K., et al. 2008, A&A, 486, 951, doi: 10.1051/0004-6361:200809724

Hong, S., Lim, D., Chung, C., et al. 2021, AJ, 162, 130, doi: 10.3847/1538-3881/ac0ce6

Hudson, M. J., & Robison, B. 2018, Monthly Notices of the Royal Astronomical Society, 477, 3869, doi: 10.1093/mnras/sty844

Husser, T. O., Wende-von Berg, S., Dreizler, S., et al. 2013, A&A, 553, A6, doi: 10.1051/0004-6361/201219058

Jordán, A., Côté, P., West, M. J., & Marzke, R. O. 2002, ApJL, 576, L113, doi: 10.1086/343759

Kostogryz, N., Shapiro, A. I., Witzke, V., et al. 2023, Research Notes of the AAS, 7, 39, doi: 10.3847/2515-5172/acc180

Kravtsov, A. V., & Gnedin, O. Y. 2005, The Astrophysical Journal, 623, 650

Kurucz, R.-L. 1993, Kurucz CD-Rom, 13

Latour, M., Husser, T. O., Giesers, B., et al. 2019, A&A, 631, A14, doi: 10.1051/0004-6361/201936242

Marigo, P., & Aringer, B. 2009, A&A, 508, 1539, doi: 10.1051/0004-6361/200912598

Marigo, P., Aringer, B., Girardi, L., & Bressan, A. 2022, ApJ, 940, 129, doi: 10.3847/1538-4357/ac9b40

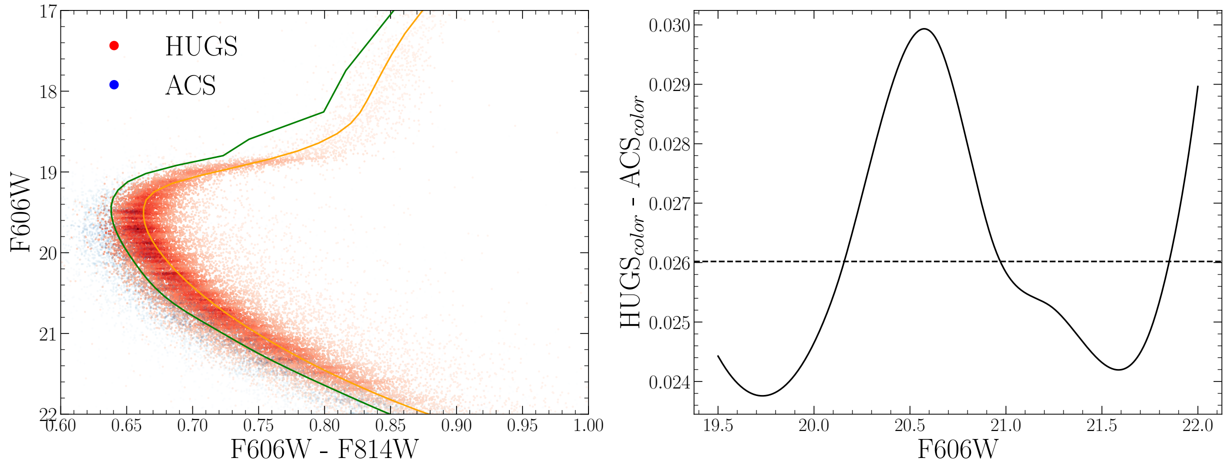

Figure 9. (left) CMD showing the photometric offset between the ACS and HUGS data for NGC 2808. CMDs have been randomly subsampled and colored by point density for clarity. (right) Mean difference between the color of the HUGS and ACS fiducual lines at the same magnitude. Note that the ACS data is systematically bluer than the HUGS data.

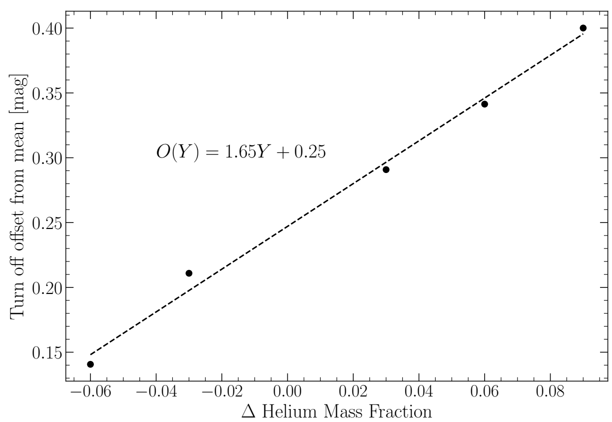

Figure 10. Main sequence turn off magnitude offset from a guage helium mass fraction (Y=0.30 chosen). All main sequence turn off locations are measured at 12.3 Gyr Should I make these contour surfaces for various ages?

Marino, A. F., Milone, A. P., Karakas, A. I., et al. 2015, Monthly Notices of the Royal Astronomical Society, 450, 815, doi: 10.1093/mnras/stv420
Milone, A. P., Piotto, G., Bedin, L. R., et al. 2012, ApJ, 744, 58, doi: 10.1088/0004-637X/744/1/58
Milone, A. P., Marino, A. F., Piotto, G., et al. 2015a, ApJ, 808, 51, doi: 10.1088/0004-637X/808/1/51
—. 2015b, MNRAS, 447, 927, doi: 10.1093/mnras/stu2446
Milone, A. P., Piotto, G., Renzini, A., et al. 2017, MNRAS, 464, 3636, doi: 10.1093/mnras/stw2531
Milone, A. P., Marino, A. F., Renzini, A., et al. 2018, MNRAS, 481, 5098, doi: 10.1093/mnras/sty2573
Pasquato, M., & Milone, A. 2019, arXiv e-prints, arXiv:1906.04983, doi: 10.48550/arXiv.1906.04983
Pedregosa, F., Varoquaux, G., Gramfort, A., et al. 2011, Journal of Machine Learning Research, 12, 2825
Peebles, P. J. E., & Dicke, R. H. 1968, ApJ, 154, 891, doi: 10.1086/149811
Peng, E. W., Ferguson, H. C., Goudfrooij, P., et al. 2011, The Astrophysical Journal, 730, 23
Piotto, G., Bedin, L. R., Anderson, J., et al. 2007, The Astrophysical Journal Letters, 661, L53, doi: 10.1086/518503
Piotto, G., Milone, A. P., Bedin, L. R., et al. 2015, AJ, 149, 91, doi: 10.1088/0004-6256/149/3/91
Plez, B. 2008, Physica Scripta Volume T, 133, 014003, doi: 10.1088/0031-8949/2008/T133/014003
Prantzos, N., Charbonnel, C., & Iliadis, C. 2007, A&A, 470, 179, doi: 10.1051/0004-6361:20077205
Renzini, A. 2008, Monthly Notices of the Royal Astronomical Society, 391, 354, doi: 10.1111/j.1365-2966.2008.13892.x
Richer, H. B., Fahlman, G. G., Buonanno, R., et al. 1991, ApJ, 381, 147, doi: 10.1086/170637
Rousseeuw, P. J. 1987, Journal of Computational and Applied Mathematics, 20, 53, doi: https://doi.org/10.1016/0377-0427(87)90125-7
Salaris, M., & Cassisi, S. 2005, Evolution of stars and stellar populations (John Wiley & Sons)
Sandage, A. R. 1953, AJ, 58, 61, doi: 10.1086/106822
Smith, G. H. 1987, Publications of the Astronomical Society of the Pacific, 99, 67, doi: 10.1086/131958
Sneden, C., Kraft, R. P., Prosser, C. F., & Langer, G. 1992, The Astronomical Journal, 104, 2121
Suntzeff, N. B., & Kraft, R. P. 1996, AJ, 111, 1913, doi: 10.1086/117930
Valle, G., Dell'Omodarme, M., & Tognelli, E. 2022, A&A, 658, A141, doi: 10.1051/0004-6361/202142454

van den Bergh, S. 2010, The Astronomical Journal, 140, 1043, doi: 10.1088/0004-6256/140/4/1043

Ventura, P., & D'Antona, F. 2009, A&A, 499, 835, doi: 10.1051/0004-6361/200811139

Ventura, P., D'Antona, F., Mazzitelli, I., & Gratton, R. 2001, ApJL, 550, L65, doi: 10.1086/319496